



**HAL**  
open science

## Electrodeposition Growth of Oriented ZnO Deposits in Ionic Liquid Media

Michal Tulodziecki, Jean-marie Tarascon, Pierre-Louis Taberna, Claude Guéry

► **To cite this version:**

Michal Tulodziecki, Jean-marie Tarascon, Pierre-Louis Taberna, Claude Guéry. Electrodeposition Growth of Oriented ZnO Deposits in Ionic Liquid Media. *Journal of The Electrochemical Society*, 2012, 159 (12), pp.D691-D698. 10.1149/2.027212jes . hal-02018952

**HAL Id: hal-02018952**

**<https://hal.science/hal-02018952>**

Submitted on 14 Feb 2019

**HAL** is a multi-disciplinary open access archive for the deposit and dissemination of scientific research documents, whether they are published or not. The documents may come from teaching and research institutions in France or abroad, or from public or private research centers.

L'archive ouverte pluridisciplinaire **HAL**, est destinée au dépôt et à la diffusion de documents scientifiques de niveau recherche, publiés ou non, émanant des établissements d'enseignement et de recherche français ou étrangers, des laboratoires publics ou privés.



## Open Archive Toulouse Archive Ouverte (OATAO)

OATAO is an open access repository that collects the work of Toulouse researchers and makes it freely available over the web where possible

This is an author's version published in: <http://oatao.univ-toulouse.fr/21747>

**Official URL:** <https://doi.org/10.1149/2.027212jes>

**To cite this version:**

Tulodziecki, Michal and Tarascon, Jean-Marie and Taberna, Pierre-Louis<sup>✉</sup> and Guéry, Claude *Electrodeposition Growth of Oriented ZnO Deposits in Ionic Liquid Media*. (2012) *Journal of The Electrochemical Society (JES)*, 159 (12). D691-D698. ISSN 0013-4651

Any correspondence concerning this service should be sent to the repository administrator: [tech-oatao@listes-diff.inp-toulouse.fr](mailto:tech-oatao@listes-diff.inp-toulouse.fr)

# Electrodeposition Growth of Oriented ZnO Deposits in Ionic Liquid Media

M. Tulodziecki,<sup>a</sup> J.-M. Tarascon,<sup>a</sup> P. L. Taberna,<sup>b</sup> and C. Guéry<sup>a,z</sup>

<sup>a</sup>Laboratoire de Réactivité et Chimie des Solides and ALISTORE European Research Institute, UMR CNRS 7314, UFR des Sciences, 80039 Amiens Cedex, France

<sup>b</sup>CIRIMAT/LCMIE and ALISTORE European Research Institute, UMR CNRS 5085, 31062 Toulouse Cedex 9, France

ZnO is a material of great interest for microelectronics because it offers a panel of attractive physical properties. It has been grown for decades as thin films from a wide variety of physical-chemical deposition techniques, most of them leading to films oriented with the polar direction perpendicular to the substrate. Here we report the electrodeposition of ZnO in ionic liquids (EMImTFSI (1-ethyl-3-methylimidazolium bis(trifluoromethylsulfonyl)imide), BMPTFSI (1-Butyl-1-Methylpyrrolidinium bis(trifluoromethylsulfonyl)imide) or BMImTf (1-butyl-3-methylimidazolium trifluoromethanesulfonate)), together with the feasibility of manipulating the growth orientation of the ZnO deposits by adding the proper co-solvent to ionic liquid. We establish solvent dielectric constant as a key parameter to tailor the deposit growth direction. Moreover, via the use of Electrochemical Quartz Crystal Microbalance (EQCM) measurements, we determine the importance of the competition between Zn<sup>2+</sup> and O<sub>2</sub> reduction to properly trigger the transport phenomena leading to the growth of ZnO. This work provides insight which can be implemented to the growth of other binary and ternary oxides deposits in ionic liquid media, a field still poorly explored.

DOI: [10.1149/2.027212jes](https://doi.org/10.1149/2.027212jes)

Room temperature Ionic Liquids (RTIL) possess many attractive chemical/physical properties. They are non-flammable, display very high thermal stability together with negligible vapor pressure and are good solvents for numerous salts and polymers.<sup>1,2</sup> Such properties are at the origin of their wide use in many research fields with an ongoing increasing interest in the synthesis of inorganic materials; such a synthesis involving either ionothermal<sup>3</sup> or electrodeposition.<sup>4</sup> Moreover by changing the nature of the cations and anions, ILs can be designed for specific applications.<sup>5</sup> Owing to their relatively high ion conductivity, ( $0.2 \Omega^{-1} \cdot \text{cm}^{-1}$ ) together with their high thermal and electrochemical stability (electrochemical window up to 4–5 V are reported), they stand as an alternative promising medium to water in the field of electrochemistry.<sup>4</sup> Such attractive characteristics have so far been widely exploited for the electrodeposition of metals and semiconductors<sup>4,6–9</sup> and very recently for binary compounds like CuS.<sup>10</sup> Additionally, control over the morphology and structure of the deposit can be achieved via tuning of the deposition conditions (temperature, wide potential window, changing cations and anions of IL, additives, mixtures of solvents, etc.<sup>4,6–10</sup>). Last, the specific interactions of IL with the electrode surface upon applied potential (which have been recently studied by a few groups) and the deposit itself may provide additional new possibilities to adjust/orient nucleation-growth mechanisms.<sup>11–15</sup>

Reduction of oxygen in Ionic Liquids is being extensively studied by many groups.<sup>16–18</sup> A common belief is that oxygen undergoes a 2 steps reduction enlisting sequentially the formation of superoxide and later on peroxide anions, both of them are stable at room temperature in ionic liquid media. Such a medium was recently exploited to electrochemically synthesize metal oxides like NiO,<sup>19</sup> ZnO<sup>20</sup> or CeO<sub>2</sub>.<sup>21</sup>

Zinc oxide is a non toxic direct wide-bandgap (3.3 eV) transparent semiconductor material widely used in the fields of chemical sensors, piezoelectric transducers, light emitting devices, photosensors and photovoltaic cells.<sup>22</sup> ZnO thin films can be deposited by several techniques such as sputtering,<sup>23</sup> pulsed laser deposition,<sup>24,25</sup> spray pyrolysis,<sup>26</sup> chemical bath deposition,<sup>27</sup> and electrodeposition,<sup>28–31</sup> the latter being the simplest. A variety of morphologies has been obtained depending on the used technique and conditions.<sup>32</sup> Physical synthesis techniques<sup>24</sup> as well as deposition from polar solvents like H<sub>2</sub>O<sup>28,30</sup> and DMSO<sup>31</sup> mostly lead to ZnO material oriented along the polar direction *z* [001] or lack of any orientation. Recently, 2 groups have shown that the preferential orientation along non-polar directions  $\langle \text{hk}0 \rangle$  can be obtained by either electrodeposition in RTIL<sup>20</sup>

or by pulsed laser deposition;<sup>25</sup> also partial tilt from *z* direction was observed by electrodeposition from a water-isopropanol mixture.<sup>33</sup> Prasad et al.<sup>33</sup> suggested that a change in dielectric constant of the solution could be responsible for the different orientations of the ZnO crystals with favorable polar orientation for solutions with high dielectric constant. This non-polar orientation is especially interesting for photovoltaic cells applications,<sup>34</sup> light emitting devices<sup>35</sup> and surface acoustic wave devices,<sup>36</sup> hence our desire to revisit the growth of ZnO in ionic liquid media following a recent paper by Azaceta et al.<sup>20</sup>

In this study we report the influence of temperature, substrate, nature of the ionic liquid, and electrochemical deposition conditions (potential and others) on the morphology and crystal structure of electrochemically grown ZnO films, and we show how the EQCM experiments can help to investigate the nucleation-growth mechanism of ZnO films. Finally the explanation of the growth of ZnO in non-polar direction will be given.

## Experimental

**ZnO deposition.**— The electrochemical bath was composed of Zn(TFSI)<sub>2</sub> (Solvionic) solution in IL either EMImTFSI (1-ethyl-3-methylimidazolium bis(trifluoromethylsulfonyl)imide), BMPTFSI (1-Butyl-1-Methylpyrrolidinium bis(trifluoromethylsulfonyl)imide) or BMImTf (1-butyl-3-methylimidazolium trifluoromethanesulfonate) ordered from Solvionic 99,9% pure (H<sub>2</sub>O < 0,005%) with the final solution being saturated with oxygen (Alphagaz, water content < 1 ppm) that was purified by passing through the column filled with dry P<sub>2</sub>O<sub>5</sub>. Prior to being used, the ILs were purified under vacuum at 75°C for 2 days; the final water content was ~6 ppm as checked by Karl Fischer measurement. High purity DMSO and toluene (stored in the glove box, water <0.1 ppm) were used for the mixture baths (1:38 volumetric ratio solvent:IL). The Zn(TFSI)<sub>2</sub> salt was chosen as zinc cation precursor in order to avoid addition of highly corrosive chlorides (ZnCl<sub>2</sub>). If not otherwise specified the concentration of zinc cations at the beginning of deposition was 0.12 M. A three-electrode set-up was used for electrochemical measurements (chronoamperometry and cyclic voltammetry) with the WE and CE electrodes oriented horizontally (only in the case of indium tin oxide substrate the configuration was vertical). Three different substrates were used as working electrodes (WE) - Platinum (Pt), Stainless steel (SS) and Indium Tin Oxide (ITO), with respective surfaces areas of  $S = 1.25 \text{ cm}^2$  for SS and Pt and  $0.75 \text{ cm}^2$  for ITO. The counter electrode (CE) was a platinum grid with high surface area ( $S \approx 2 \text{ cm}^2$ ). The Ag wire was used as the pseudo reference electrode due to its stability at high temperature. All the values of potential will be given versus the pseudo Ag reference electrode if not otherwise specified. Prior to being used, the WE and

<sup>z</sup>E-mail: [claud.guery@u-picardie.fr](mailto:claud.guery@u-picardie.fr)

CE electrodes were cleaned in 2M nitric acid in ultrasonic bath for 1h, and then intensively rinsed with distilled water and ethanol. All the components of the cell were dried in the oven (50°C) for 2 hours before the experiment. The cell was immersed in the oil bath while the temperature was controlled with a  $\pm 2^\circ\text{C}$  difference between heating and deposition bath.

The electrochemical measurements were carried out with Autolab PGSTAT 30 potentiostat (Eco Chemie BV). All the CVs measurements were performed starting from the OCV with a reduction scan followed by the oxidation one. The potential range for electrodeposition was chosen in the range of IL electrochemical stability window ( $-0.8$  to  $-1.9$  V versus Ag) and the electrodeposition time was selected according to other conditions (1h to 4h). The electrodeposition was performed at 2 different temperatures 20 and  $100^\circ\text{C}$ . The bath was bubbled with oxygen before and during the measurement. The obtained deposits were thoroughly rinsed with acetone and soaked in dichloromethane for 4h in order to remove adsorbed IL from the surface.

The morphology and crystal structure of deposits were analyzed using Philips XL 30 field emission gun FEG microscope and Bruker D4 diffractometer with copper radiation, respectively. The Transmission electron microscopy measurements were performed on FEI TECNAI F20 S-TWIN microscope.

The EQCM measurements were carried out using commercial SEIKO microbalance with AT-cut 9 MHz quartz covered with platinum on both sides. The electroactive geometric surface area was equal to  $S = 0.196\text{ cm}^2$ . A simultaneous measurement of the quartz frequency and resistance was done in order to subtract the influence of bath viscosity and density on the frequency change as it was observed in AgTFSI solution.<sup>37</sup> Prior to the measurement, the EQCM was calibrated, with 0.05M solution of AgTFSI in EMImTFSI at  $100^\circ\text{C}$  with  $2\text{ mV} \cdot \text{s}^{-1}$  scanning rate, to determine proportionality constant ( $\Delta m = C \cdot \Delta f$ )<sup>38</sup> between the change of quartz frequency ( $\Delta f$ ) and change of deposited mass ( $\Delta m$ ). A constant C value of 1.065 ng/Hz close to the theoretical one of 1.068 ng/Hz was found suggesting that issues regarding viscosity of the bath or roughness of the substrate can be neglected. So, to analyze the EQCM data, the function  $M/z$  (molar mass over number of exchanged electrons) was simply calculated according to equation 1 and Faraday's laws of electrolysis, assuming that the reaction efficiency is near 100%.

$$\frac{M}{z} = FC \frac{d\Delta f}{dQ} \quad [1]$$

Under such conditions, the expected value of  $M/z$  for the growth of ZnO, which relies on a  $2\text{ e}^-$  process, is  $41\text{ g} \cdot \text{mol}^{-1}$ . The CVs (scanning rate  $2\text{ mV/s}$ ) measurement was performed in 0.12 M Zn(TFSI)<sub>2</sub> solution in EMImTFSI at  $100^\circ\text{C}$  under O<sub>2</sub> atmosphere. During the experiment, the oxygen was only flushed over the solution not to disturb microbalance performances.

## Results and Discussion

*CV of bath components.*— We initially surveyed the influence of temperature and concentration of the zinc cations on the reduction of oxygen and found, in agreement with Azaceta et al., that both cations content and temperature enhance the reduction of oxygen. Since our studies were performed with different substrates using different solutions, we judged useful to report the CV curves for the bath components separately and all together at  $100^\circ\text{C}$  on Pt substrate.

Figure 1 presents the CVs curves of bath components separately and all together. The reduction stability of EMImTFSI was limited to  $-2.0$  V (Fig. 1a, black curve). For the pure IL saturated with O<sub>2</sub> (Fig. 1b, red curve) two reduction waves were observed, one (A) centered at  $E = -1$  V (onset at  $E = -0.7$  V, see inset on Figure 1a) and a second (B) at  $E = -1.4$  V, consistent with the two-step oxygen reduction process reported in the literature.<sup>16</sup> For the 0.12 M Zn(TFSI)<sub>2</sub> solution under Ar atmosphere (Fig. 1c, green curve) we observed a single reduction peak (D) at  $E = -1.23$  V due to the reduction of Zn<sup>2+</sup> to Zn<sup>0</sup> with, however, a small preceding wave (C) which can be due to the underpotential

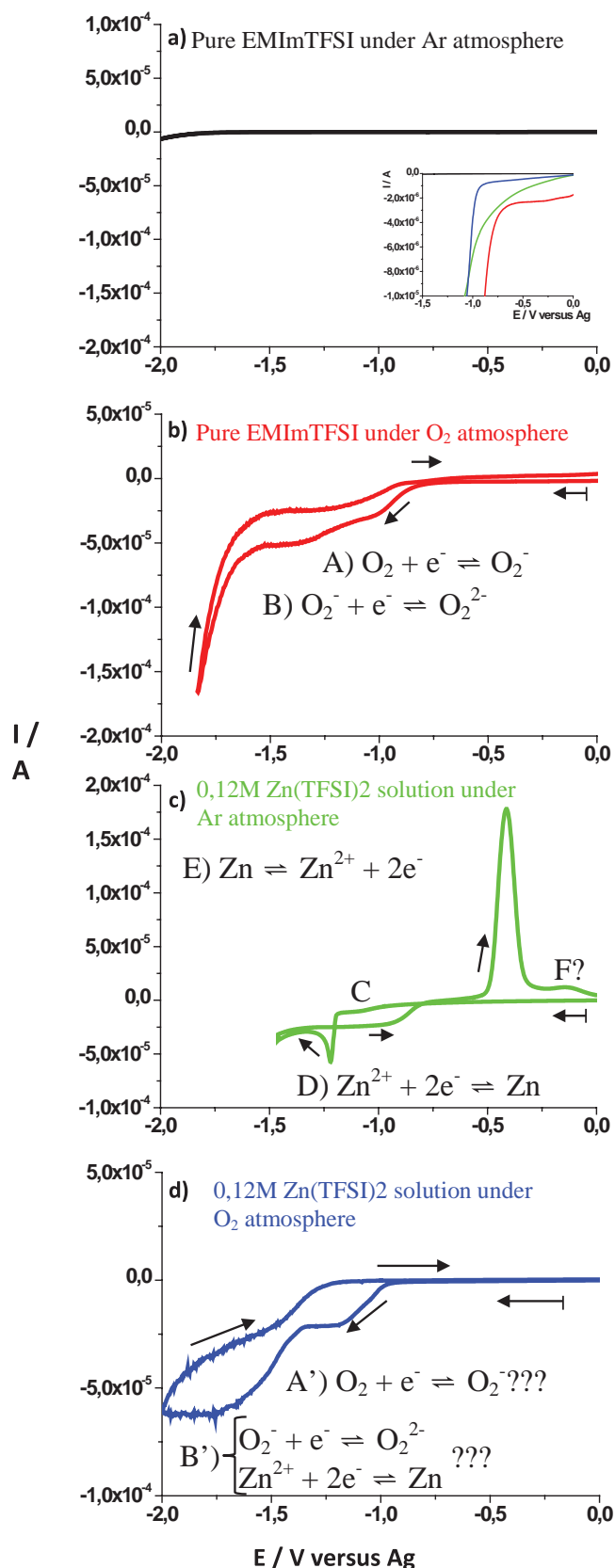


**Figure 1.** CVs curves of electrochemical bath components separately and all together. (a) black curve – pure ionic liquid under Argon atmosphere, (b) red curve – pure ionic liquid under oxygen atmosphere, (c) green curve –0,12 M Zn(TFSI)<sub>2</sub> solution under Ar atmosphere, (d) blue curve –0,12 M Zn(TFSI)<sub>2</sub> solution under O<sub>2</sub> atmosphere. T =  $100^\circ\text{C}$ , WE – Pt, CE – Pt, RE – Ag, scan rate  $50\text{ mV} \cdot \text{s}^{-1}$ . The inset - magnification of the reduction step for all the curves.

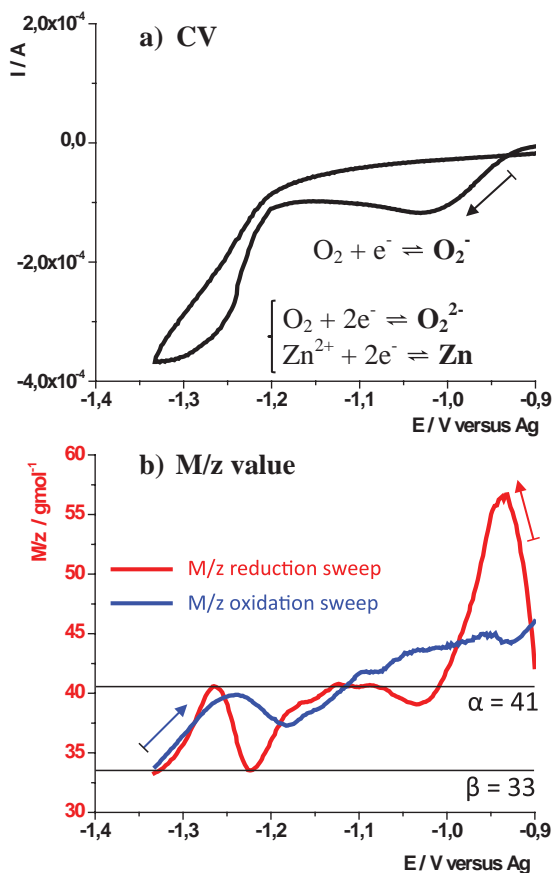


**Figure 2.** EQCM measurements: (a)  $I$  versus  $E$  curve, (b)  $M/z$  function versus potential, red (reduction sweep) and blue (oxidation sweep) curve. 0.12 M  $\text{Zn}(\text{TFSI})_2$  solution under  $\text{O}_2$  atmosphere.  $\alpha$  corresponds to  $\text{ZnO}$  deposition,  $\beta$  corresponds to  $\text{Zn}$  deposition.  $T = 100^\circ\text{C}$ , WE – Pt on quartz, CE – Pt, RE – Ag, scan rate  $2 \text{ mV} \cdot \text{s}^{-1}$ .

deposition of  $\text{Zn}$ . Two peaks located at  $E = -0.41$  and  $-0.13 \text{ V}$  (E and F, respectively) are observed on oxidation. Although we don't have a clear explanation, these two peaks, whose amplitude ratio was found to vary with the number of scans (annex Fig. 1\*), could be rooted in either the existence of two zinc morphologies with different oxidation energies (as suggested by Abbott et al. based on simultaneous in situ AFM and EQCM measurements)<sup>39,40</sup> or different kinds of complexation of  $\text{Zn}^{2+}$  cations by  $\text{TFSI}^-$  anions. Last, when  $\text{O}_2$  and  $\text{Zn}^{2+}$  are present in the solution (Fig. 1d, blue curve), we noted the appearance of two reduction waves centered at  $E = -1.20$  and  $-1.70 \text{ V}$  (A' and B' respectively) and no oxidation signals. The first reduction wave is shifted to negative values as compared to what was found for  $\text{O}_2$  in pure EMImTFSI (Fig. 1b, red curve) and this independently of the substrate SS or ITO (annex Fig. 3a, 3b\*) that we were using. It could be caused by a change of physical parameters of IL in the vicinity of WE (viscosity, change in double layer) when zinc cations are added.

To grasp further insight into the nature of those two reduction peaks we decided to carry EQCM measurements while performing cyclic voltammetry at a rate of  $2 \text{ mV/s}$  (Fig. 2). Such a slow rate was purposely used to obtain better resolution (because of lower ohmic drop) as well as a good microbalance response. Figures 2a and 2b represent CVs curve and change of  $M/z$  value versus potential, respectively. At the beginning of reduction (Fig. 2b red curve) a sharp increase in  $M/z$  value ( $M/z = 56$ ) is observed, most probably due to the nucleation process (formation of deposits) as well as adsorption of the ions on to the electrode.<sup>41</sup> Once the thin compact layer is formed, the  $M/z$  stabilizes at a value of  $41 \text{ g} \cdot \text{mol}^{-1}$ , as expected for zinc oxide deposition. This means also that the reaction is almost 100% efficient as in our previous assumption. Additionally, during the first reduction

peak a drop of resistance of about 20 ohms is observed (annex Fig. 2b\*), and it corresponds to a decrease in viscosity/density of the solution near the electrode surface caused by depletion of zinc cations, as mentioned in the experimental part. According to the final deposition product  $\text{ZnO}$  ( $M/z = 41 \text{ g} \cdot \text{mol}^{-1}$ ) we could assign the first reduction peak to the formation of superoxide ions as indicated on Figure 2a. Turning to the second reduction peak a “sinusoidal-type” variation of the  $M/z$  value is observed. It is concomitant with the appearance of a slightly gray deposit, indicating the deposit of metallic zinc ( $M/z = 33$  for the 2 electron reduction reaction of Zinc cations). The variation of the  $M/z$  value between 33 and 41 further indicates an alternating process of reduction of zinc cations to metallic zinc and oxygen to peroxide ions as indicated on Figure 2a. On the reverse sweep a very small and broad oxidation wave was observed while the gray color of deposit diminished. The absence of well-defined oxidation peak for  $\text{Zn}$  means that the reduction/oxidation process of  $\text{Zn}/\text{Zn}^{2+}$  couple in the presence of oxygen is poorly reversible, probably due to the increasing amount of a nearly insulating  $\text{ZnO}$  deposit.

The above experimental protocol was implemented to study the effect of changing the nature of the substrate, the nature of the ionic liquid, the temperature or the solvents. Whatever the modifications made, we shortly found that the overall shape of the CV curve collected on Pt substrate was preserved (annex Fig. 3, 4\*) with therefore minor changes on the onset positions and amplitudes of the redox peaks. Such shifts on the onset potentials of the reduction peaks are summarized, for instance, in annex (Tables I, II and III\*) for different conditions.

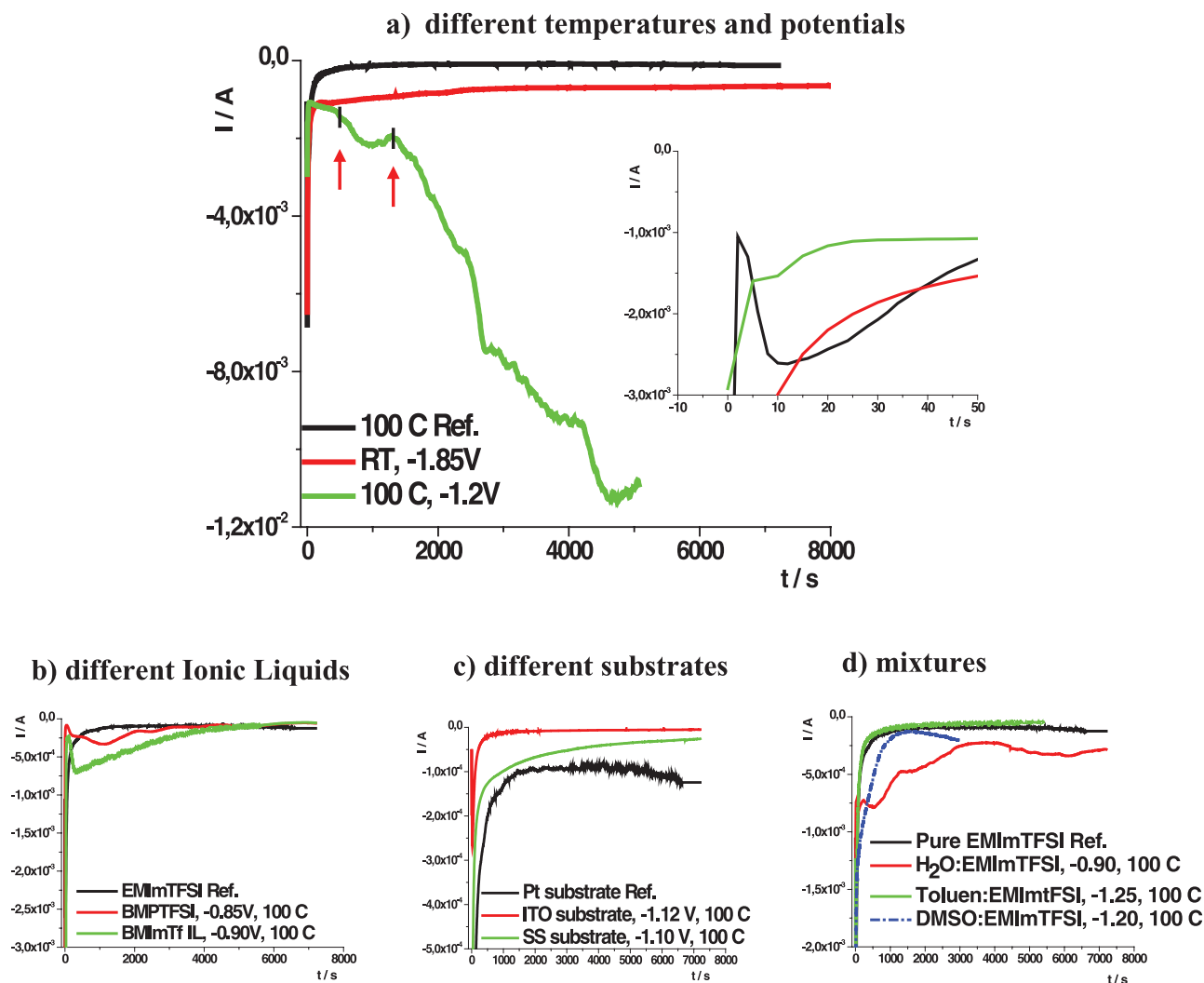
**Potentiostatic electrodeposition.**— All the electrodeposition conditions are summarized in Table I. From now on if not otherwise specified, the deposition conditions: 0.12 M  $\text{Zn}(\text{TFSI})_2$  solution in EMImTFSI,  $T = 100^\circ\text{C}$ ,  $E = -1.00 \text{ V}$ ,  $t = 2 \text{ h}$  will be considered as the reference conditions. Based on EQCM measurement we limited the potential deposition range (for deposition at  $100^\circ\text{C}$ ) from  $-0.8 \text{ V}$  to  $-1.2 \text{ V}$  to avoid electrodeposition of metallic Zinc, at this potential range formation of super oxide occurs. In case of mixtures DMSO and toluene with IL the experiment had to be terminated before planned time due to a change in bath color.

Figure 3a (black curve) represents the current profile of chronoamperometric experiment at reference conditions. We initially observed a huge increase in current which then slightly decreased prior to stabilizing and reaching steady state. This is the typical characteristic of a nucleation-growth mechanism with the current downturn corresponding to the time at which the grains start to grow (e.g., decrease in the current is due to increase in surface area).<sup>40</sup> Once the thin layer is created there is a stabilization of the current most likely due to mass transport limitation (e.g., diffusion of  $\text{O}_2$  toward the electrode).

The current profile for deposition at  $100^\circ\text{C}$  at lower potential ( $-1.20 \text{ V}$ ) significantly differs (Fig. 3a, green curve) since the characteristic valley on the  $I = f(t)$  is no longer observed. In contrast, after 400 s (as indicated by black lines and arrows) there is a high decrease in current, probably due to deposition of  $\text{ZnO}$  with different

**Table I. Electrodeposition conditions for all the baths. The deposit obtained from the conditions marked with star \* is a reference deposit.**

mixture	Chronoamperometric deposition			T / s
	Substrate	Temp / °C	E / V	
EMImTFSI*	Pt	100	-1.00	7200
EMImTFSI	Pt	RT	-1.85	14400
EMImTFSI	Pt	100	-1.20	5100
EMImTFSI	SS	100	-1.10	7200
EMImTFSI	ITO	100	-1.12	7200
BMPTFSI	Pt	100	-0.85	7200
BMImTf	Pt	100	-0.90	7200
$\text{H}_2\text{O}$ : EMImTFSI	Pt	100	-0.90	7200
DMSO: EMImTFSI	Pt	100	-1.20	3000
Toluene: EMImTFSI	Pt	100	-1.25	5500



**Figure 3.** Current profiles of chronopotentiometric experiments. (a) different temperatures and potential, (b) different Ionic Liquids, (c) different substrates, (d) mixtures of IL with other solvents. Inset represent the beginning of the deposition.

morphologies, and then after 1500 s (see arrow on the curve) a second very sharp decrease in current most likely due to the deposition of metallic zinc. Surprisingly this behavior is no longer observed when the deposition proceeds at RT and lower potential ( $-1.85$  V) since the  $I = f(t)$  curve shows a diffusion limited current process (Fig. 3a red curve) associated to an excess of oxygen ( $O_2^{x-}$ ) which captures  $Zn^{2+}$  prior to being reduced. Most probably at such low potential we have the formation of peroxide ions instead of superoxide that changes the mechanism of ZnO synthesis compared to the deposition at 100 C at potentials higher than  $-1.2$  V.

Changes in the nature of the ionic liquids are found to affect the overall shape of the current profile (Fig. 3b). For instance, with a BMPTFSI and BMImTf solution, the process spreads over time as the initial valley in the current profile prior stabilization takes more than 2000s while for EMImTFSI solution it is a few hundreds seconds (200s). The time difference effect is most likely nested in the specific interaction of IL with the surface of newly deposited particles and substrate that probably differs according to the type of IL.

Turning to the nature of the substrate we found that it had a greater impact on the current profile (Fig. 3c) since, for instance, the characteristic valley on the I-t curve for nucleation and growth mechanism is not very well defined in the case of SS substrate (Fig. 3c green curve).

Last, we experienced that the addition of extra solvent as toluene or DMSO did not influence the shape of the current profile (Fig. 3d). This is in contrast with the addition of  $H_2O$  (Fig. 3d red curve) which

slightly changes the shape of the current profile with i) the absence of valley on  $I = f(t)$  curve, and ii) the appearance of a wavy current profile which we assigned to changes in the morphology of the deposits as it will be discussed later.

*Deposit morphology.*— Figures 4, 5 present the SEM images of individual deposits with at first the reference deposit, obtained at 100°C with a 0.12 M  $Zn(TFSI)_2$  solution in EMImTFSI when clamping the potential at  $-1.00$  V for 2 hours, and which is transparent. It is composed of a thin compact layer ( $\sim 500$ nm) with, in addition, 200–300 nm grains on top as can be seen in Figures 4a and 4b. It is worth noting that cracks are not initially present in the film but are developing upon long beam exposure (annex Fig. 5\*). To grasp more insight in the primary particles we carried TEM measurements which indicate that the deposit is made of very small crystallites (6 nm) as deduced by HRTEM measurement (annex Fig. 6\*). From EDX we also spotted peaks associated to F and S suggesting the presence of residual ionic liquid that could not be fully eliminated even after several washings with methane dichloride. This does not come as a total surprise since we previously experienced a similar surface contamination for all the powders we have so far prepared by ionothermal synthesis even after copious washing either in dimethyl chlorine or ethyl acetate.<sup>42</sup>

Lowering the electrodeposition potential to  $-1.2$  V leads to an inhomogeneous deposit (Fig. 4c, 4d) composed of 3 different layers

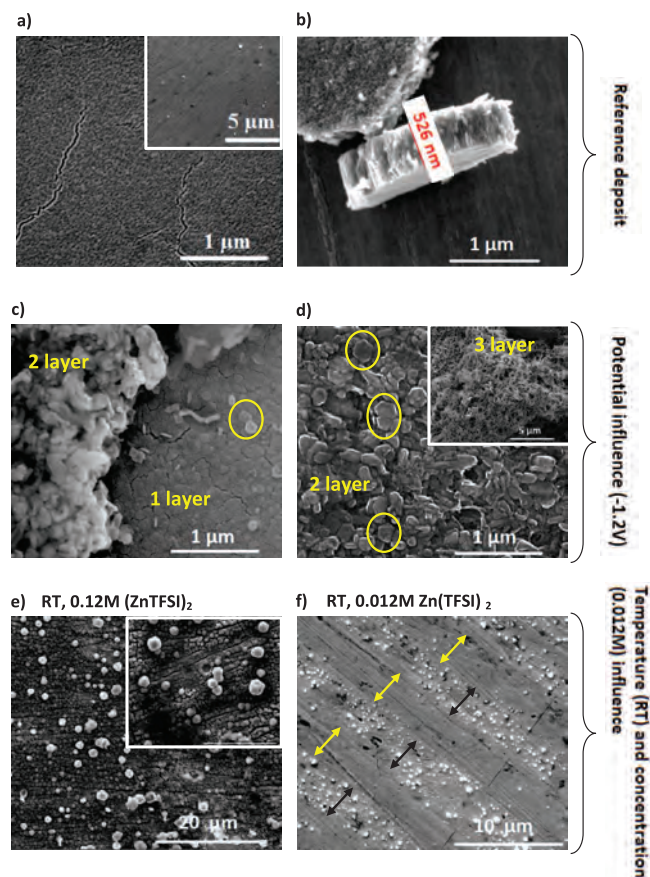


**Figure 4.** SEM images of particular deposits: (a,b) 100°C, -1.00 V, 0.12 M Zn(TFSI)<sub>2</sub> in EMImTFSI on Pt (reference deposit); (c,d) 100°C, -1.20 V, 0.12 M Zn(TFSI)<sub>2</sub> in EMImTFSI on Pt; (e) RT, -1.85 V, 0.12 M Zn(TFSI)<sub>2</sub> in EMImTFSI on Pt; (f) RT, -1.85 V, 0.012 M Zn(TFSI)<sub>2</sub> in EMImTFSI on Pt.

as suggested by the current profile (Fig. 3a green curve). Departing from the Pt substrate we first found i) a compact thin layer of ZnO ~ 500 nm thick (layer 1, Fig. 4c) which is alike the one grown at -1.0 V, ii) another compact layer of ZnO grains with hexagonal shape (layer 2, Fig. 4c and 4d), and iii) last a non adhesive sponge-like layer composed of Zn metal (layer 3, Fig. 4d inset). Such an inhomogeneous deposition is believed to be due to the rapid decrease in oxygen concentration near the sample deposit surface. This is consistent with early reports which mentioned that the concentration of the ingredients within the bath has a huge influence on the deposit morphology.<sup>30</sup>

Turning to the room temperature deposition at -1.85 V in 0.12 M Zn(TFSI)<sub>2</sub> in EMImTFSI, we obtained (Fig. 4e) a grayish layer deposit which shows cracks together with a copious amount of 1 μm big grains. Interestingly, by decreasing the concentration of Zn cations by a factor of 10, we obtained a different morphology with namely the alignment of ZnO grains in a strip-like shape with equal spacing (5 μm) between strips (see arrows Fig. 4f). Such a pattern, which we found to be intrinsic to the deposit growth, can be nested in a specific interaction of IL with substrate (coupling of the platinum wave functions with the π orbitals of the imidazolium cations as early mentioned<sup>11-15</sup>) favoring such an alignment. The local arrangement of IL (e.g. liquid-crystal type) could cause the orientation in deposit too. This is possible since we early demonstrated in our ionothermal synthesis work the feasibility of using ionic liquids as structural directing agent.<sup>43</sup>

Such a specific IL-substrate interaction seems to disappear with temperature since we found that at 100 °C neither the type of the IL (Fig. 5a and 5b) nor the substrate influence (Fig. 5c and 5d) significantly affect the morphology of the deposits with the exception of the deposit density. In all the cases a thin transparent layer topped with a few ZnO grains was obtained as in the case of the reference deposit.

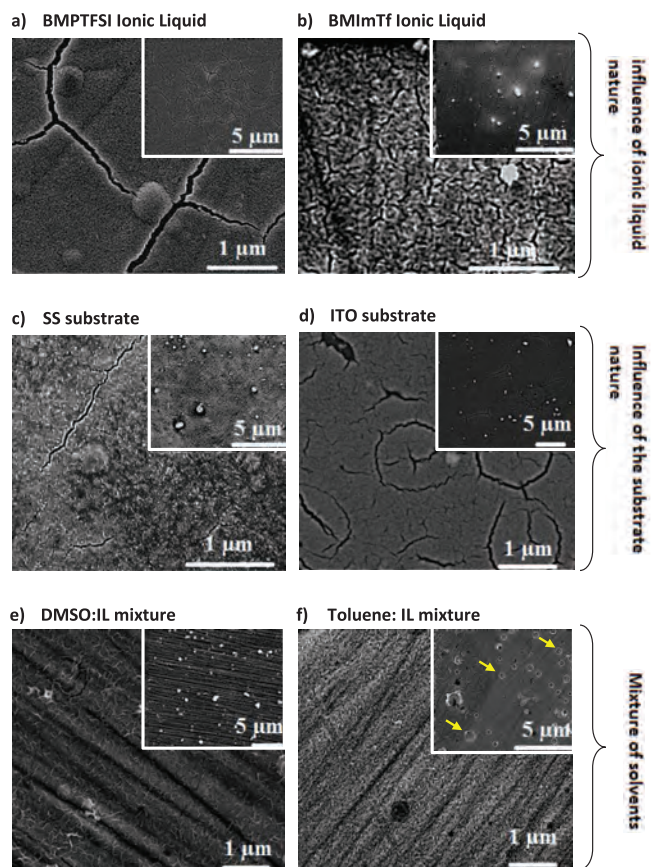


**Figure 5.** SEM images of particular deposits: (a) 100°C, -0.85 V, 0.12 M Zn(TFSI)<sub>2</sub> in BMPTFSI on Pt, (b) 100°C, -0.90 V, 0.12 M Zn(TFSI)<sub>2</sub> in BMImTf on Pt (c) 100°C, -1.10 V, 0.12 M Zn(TFSI)<sub>2</sub> in EMImTFSI on SS, (d) 100°C, -1.12 V, 0.12 M Zn(TFSI)<sub>2</sub> in EMImTFSI on ITO, (e) 100°C, -1.20 V, 0.12 M Zn(TFSI)<sub>2</sub> in DMSO:EMImTFSI on Pt, (f) 100°C, -1.25 V, 0.12 M Zn(TFSI)<sub>2</sub> in toluene:EMImTFSI on Pt.

Last, electrodeposition was also carried out with the additions of many solvents, such as toluene, DMSO, H<sub>2</sub>O to our ionic liquid media. In the case of DMSO:IL mixture the 250 nm deposit reveals many valleys and hills as well as some cracks (Fig. 5e). In contrast a lower surface roughness was observed for the 300 nm deposits grown in a toluene:IL mixture (Fig. 5f) with therefore the presence of hole-like spots, which could originate from a partial evaporation of trapped toluene molecules (Fig. 5f inset). The morphology of the deposits grown in H<sub>2</sub>O:IL mixture (annex Fig. 7\*) totally changed, and it is composed of grains with very sharp edges which create a compact layer. Nevertheless, by tuning the deposition time we found out that transparent ZnO thin film alike in our reference can be obtained.

**Crystal Structure.**— Figure 6, 7 present the XRD patterns of all deposits as well as the projection of stack of ZnO unit cells along polar direction. The amplitude of the peaks is very low with respect to the substrate ones due to tiny amounts of deposit. Moreover, they are broad as compared to commercial ZnO powder confirming the presence of small crystallites as indicated by microscopy. For the reference deposit (Fig. 6b), many of the peaks expected from the ZnO hexagonal crystal structure are absent suggesting a preferential orientation of the deposit. The appearance of the (100) and (110) Bragg peaks together with the absence of (002) indicates a high orientation of the reference deposit in (hk0) direction.

We found that the orientation of the deposit is lost (Fig. 6b) when the deposition is performed at lower potential (-1.2 V) and 100°C, due to the non-homogeneity of the deposit (3 layers). The samples prepared at RT were featureless (Fig. 6b) due to poor crystallinity as

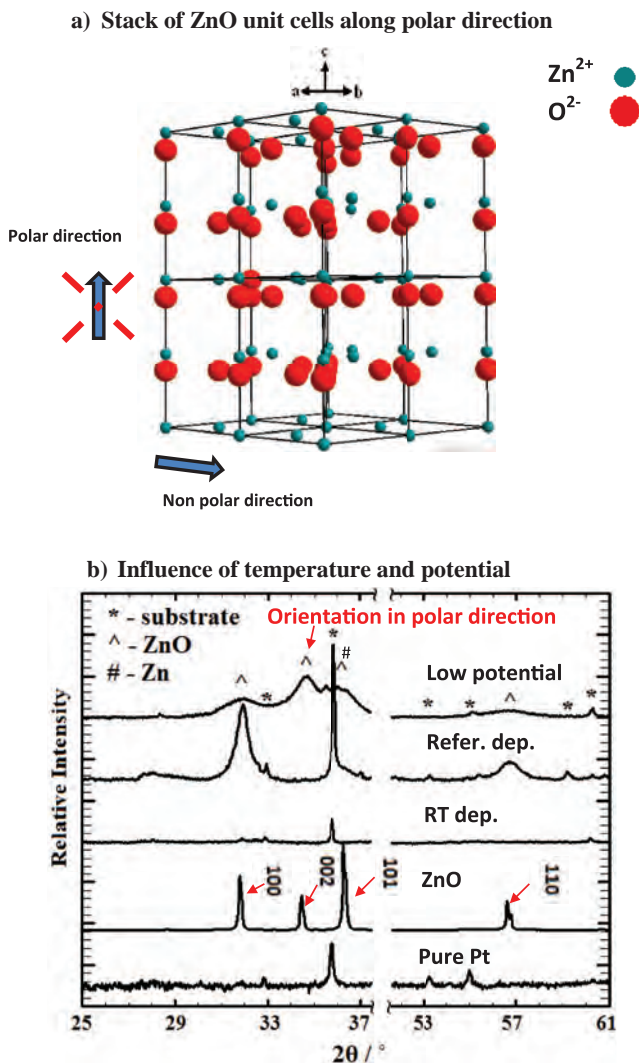


**Figure 6.** (a) Projection of stack of ZnO unit cells along z direction. (b) XRD patterns of deposits and substrates, (from the bottom to top), Pt substrate; ZnO powder; RT deposit from EMImTFSI solution; 100°C deposit from EMImTFSI on Pt at  $-1$  V; 100°C deposit from EMImTFSI on Pt at  $-1.2$  V.

confirmed by the SAED patterns which are quite diffused. Nevertheless, the ED patterns were found to improve upon long exposure to electron beam implying a high temperature-driven crystallization.

The non-polar orientation ( $(hk0)$  growth direction) remained unchanged whatever the nature of IL or substrate we have been using (Fig. 7a and 7b). This suggests that this specific orientation is most likely nested in the nature of the solvent which could affect the dielectric constant (Imidazolium and pyrrolidinium based IL possess very low dielectric constant value in range of 10–15<sup>44</sup>) or viscosity of the electrolytic bath. To test this hypothesis we have performed electrodeposition from mixtures of solvents starting with non-aqueous ones. The XRD powder pattern collected for a deposit grown in DMSO:IL mixture (increase in dielectric constant value while maintaining high viscosity) reveals the presence of the (002) Bragg peak which implies the loss of the non-polar growth direction (Fig. 7c). In contrast, films prepared from toluene:IL mixture (decrease in viscosity while maintaining low dielectric constant) are alike those obtained in IL alone (Fig. 7c). This indirectly suggests that the dielectric constant of the solvent plays a significant part in controlling deposit orientation.

Now turning to H<sub>2</sub>O:IL media, the results are quite different (annex Fig. 8<sup>\*</sup>). The XRD pattern shows 4 peaks out of which two only match the  $2\theta$  positions corresponding to the (100) and (110) Bragg

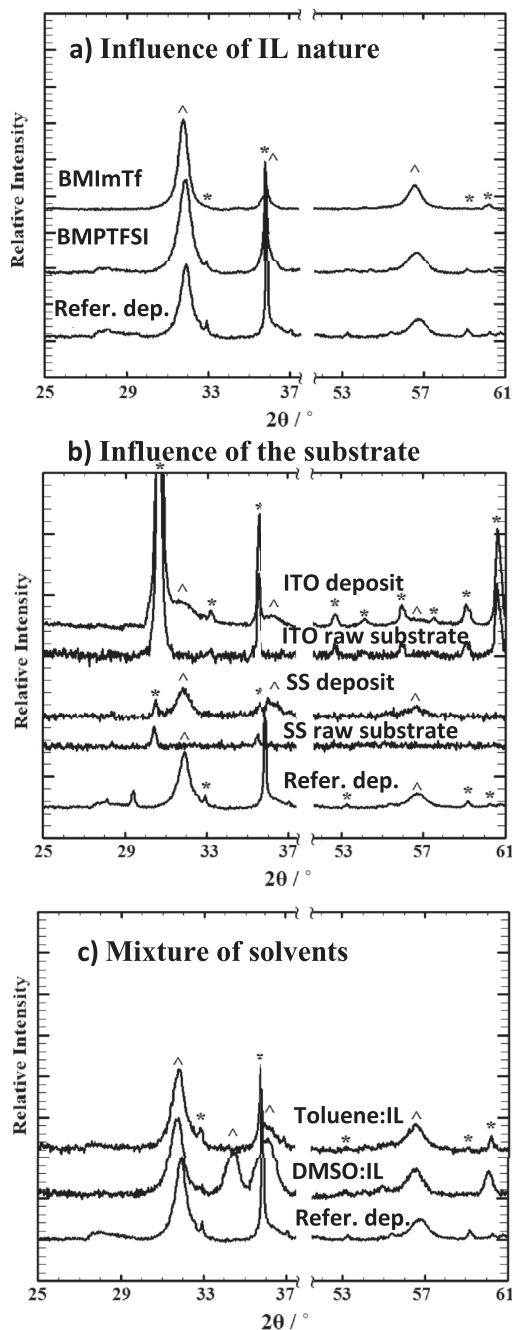


**Figure 7.** XRD patterns of deposits and substrates: (a) (from the bottom to top) different IL deposits, EMImTFSI; BMPTFSI; BMImTf. (b) different substrates, 100°C deposit from EMImTFSI on Pt; SS raw substrate; deposit on SS; ITO raw substrate; deposit on ITO. (c) mixtures of IL with other solvents, 100°C deposit from EMImTFSI on Pt; IL:DMSO; IL:toluene.

peaks of hexagonal ZnO. The amplitude of the two remaining ones, which we identified as corresponding to zinc hydroxide Zn(OH)<sub>2</sub> from both IR and XRD measurements, were found to change with the electrolytic bath conditions. We found that pure Zn(OH)<sub>2</sub> thin films can be obtained at RT from H<sub>2</sub>O:IL mixture; such a phase was shown to transform upon heat-treatment at 200°C into hexagonal ZnO keeping its non polar orientation, giving us a second route to obtain this specific orientation. Moreover for deposition at 100 °C the longer the bath was kept at 100°C the lower the amount of Zn(OH)<sub>2</sub> was obtained, due to evaporation of water from the bath. After 2hrs preheating, only pure ZnO could be deposited.

## Discussion

ZnO is mainly grown in the polar direction via physical deposition techniques. This contrast with our present work which indicates that ZnO thin film deposits can be grown in the non-polar direction via electrodeposition provided that we manipulate the dielectric constant of electrolytic bath composition. It now pertains to us to provide a rational explanation to account for such an observation and to return to the EQCM measurements.

The sinusoidal variation of  $M/z$  value during the second reduction wave (Fig. 2b) suggests that the reactions taking place at the electrode are ruled by transport phenomena, hence the importance of the huge difference in diffusion coefficients of the reacting species  $Zn^{2+}$  ( $D_{RT} = \sim 10^{-12}$ ),<sup>45</sup>  $O_2$  ( $D_{RT} = \sim 10^{-10}$ )<sup>17</sup> and intermediate species  $O_2^-$  ( $D_{RT} = \sim 10^{-11}$ )<sup>17</sup> as well as difference in concentrations  $O_2$  ( $C_{RT} = 0.005 M^{17}$ ), Zn ( $C = 0.12 M$ ), making the diffusion of molecular oxygen much faster than zinc cations. It results that, depending on the chosen deposition potential, which can be either before reduction of zinc cations (high potential) or after the onset of zinc reduction (low potential), two scenarios can be envisioned.

At high potential ( $-1.0 V$ ) and  $100^\circ C$  the growth of ZnO can be explained as follows. Firstly, the produced superoxide accumulates near the electrode due to its low diffusion coefficient as compared to molecular oxygen, and this is experimentally confirmed by the small lag between the frequency change and beginning of oxygen reduction observed during EQCM measurements (annex Fig. 2a\*). Later superoxide ions  $O_2^-$  react with  $Zn^{2+}$  causing its depletion near the electrode (as indicated by drop in resistance annex Fig. 2b\*) with the end result being a transportation controlled deposition of compact ZnO layer. Occasionally, we have additional growth of ZnO grains over this thin layer which can be due to either changes in the oxygen concentration at the vicinity of the electrode or changes in the conductivity of the active surface, via non homogeneity of thicknesses, since ZnO is highly resistive. The reduction of  $Zn^{2+}$  cannot occur since the potential is too high.

For the  $100^\circ C$  deposition at low potential ( $-1.2 V$  where reduction of zinc cations is possible Fig. 1c), even though the concentration of Zinc cations is around 25 times higher than molecular oxygen ( $C_{O_2} = 0.005 M^{17}$ ), the first steps of electrodeposition are similar to the high potential deposition. At the beginning, only  $O_2$  is reduced and the thin layer of ZnO is formed. After a certain time (400s) a thin layer is formed (Fig. 3a) and the growth of second ZnO morphology starts; further deposition of Zn occurs (after 1500 s) due to a decrease in concentration of oxygen in the vicinity of the electrode (the flux of oxygen is not sufficient to react with all  $Zn^{2+}$  near the double layer). This is also confirmed by EQCM measurements (Fig. 2), where alternative reactions of zinc and oxygen reduction occur, because the  $M/z$  value varies between 41 and 33 at low potentials. In contrast, when the deposition is done at RT no zinc reduction occurred at very low potential ( $-1.85 V$ ), even after a long time (4h), indicating that the  $Zn^{2+}$  reduction is totally suppressed (Fig. 3a). Changes in the concentration of molecular oxygen in the bath at low and high temperatures, change of the reaction mechanism (formation of peroxides that may form a blocking diffusion layer) as well as changes in the coordination of Zinc cations upon heating could be at the origin of such a difference.

Turning to the deposit growth direction we show that it can be switched from polar (along (001)) to non polar (along (hk0)) depending upon the composition of the electrodeposition bath. It was earlier reported that highly polar solvents like water,<sup>30</sup> DMSO<sup>31</sup> or mixture of DMSO with IL (as we reported) lead to deposits either oriented in the polar direction or with random orientation. Here we have pushed this observation further by showing that solvents with low dielectric constant EMImTFSI ( $\epsilon = 12.0$ )<sup>44</sup> and more so toluene ( $\epsilon = 2.38$ ) lead to deposits oriented along the non-polar direction, clearly stressing the importance of solvent dielectric constant in ruling the ZnO growth direction. Moreover, we show that using ionic liquid conjointly with another solvent such as toluene enables to overcome the poor ionic liquid viscosity so as to improve transfer phenomena. Needless to say that dilution effect (IL + Solvent) can also influence the coordination

of the zinc cations and hence drastically affect the electrodeposition process as it is observed with the addition of water.

## Conclusions

We have reported the electrodeposition growth in ionic liquid media of ZnO deposits on Pt, SS, ITO substrates. From combined XRD and SEM/TEM measurements we have shown that neither the substrate, cation nor anion character of IL (possessing low dielectric constant value) does influence the morphology or crystal structure of the deposit in contrast to both deposition potential and temperature, with for the latter amorphous deposits for films grown at RT as opposed to well crystalline and (hk0) oriented deposits for  $100^\circ C$  grown films. We have provided direct evidence, via well selected solvent additives as DMSO and toluene, having different dielectric constants ( $\epsilon = 46.7$  and  $\epsilon = 2.38$ , respectively), that the film growth orientation is mainly governed by solvent dielectric constant. So it results that mixtures of ILs-solvents can be manipulated to orient on the demand the growth direction of the ZnO deposits, provided the absence of water traces usually promoting the deposition of metal hydroxide.

More broadly we have shown how EQCM measurements can be used to follow the nucleation-growth mechanism process and to probe the type of reactions taking place at the electrolyte-substrate interface. When the electrodeposition is done at low potential, such measurements have shown competing processes associated to the reduction of zinc cations and molecular oxygen, with the reduction of zinc starting when the concentration of oxygen reaches a low critical value. Needless to say that the huge difference in the diffusion coefficients and concentration of molecular oxygen and zinc cations, is a key in determining the reacting schemes leading to the formation of ZnO deposits, with the feasibility of having different reacting pathways depending on the growth temperature and deposition potential. The use of further characterization techniques such as in situ STM, AFM and EQCM is immediately apparent to grasp further details on the ZnO growth mechanism depending on the type of ionic liquid or water-based electrolytic baths. Overall we hope that this work will serve as an impetus to implement the electrodeposition technique to the growth of various binary and ternary oxides as we are presently doing with success since copper, cobalt and manganese oxides have already been grown as it will be reported in a coming paper.

## Acknowledgment

The authors thank Prof. L. Dupont (LRCS, Amiens) for the TEM measurements as well as P. Simon for fruitful discussions.

## References

1. M. Armand, F. Endres, D. R. MacFarlane, H. Ohno, and B. Scrosati, *Nat. Mater.*, **8**, 621 (2009).
2. S. Keskin, D. Kayrak-Talay, U. Akman, and O. Hortacsu, *J. Supercrit. Fluid.*, **43**, 150 (2007).
3. N. Recham, J. N. Chotard, L. Dupont, C. Delacourt, W. Walker, M. Armand, and J. M. Tarascon, *Nat. Mater.*, **9**, 68 (2010).
4. F. Endres, D. MacFarlane, and A. Abbott, *Electrodeposition from Ionic Liquids*, Wiley-VCH Verlag GmbH and Co. KGaA (2008).
5. M. J. Earle and K. R. Seddon, *Pure Appl. Chem.*, **72**, 1391 (2000).
6. W. Simka, D. Puszczczyk, and G. Nawrat, *Electrochim. Acta*, **54**, 5307 (2009).
7. F. Endres, M. Bukowski, R. Hempelmann, and H. Natter, *Angew. Chem., Int. Ed.*, **42**, 3428 (2003).
8. W. Freyland, C. A. Zell, S. Z. El Abedin, and F. Endres, *Electrochim. Acta*, **48**, 3053 (2003).
9. C. Lecoeur, J. M. Tarascon, and C. Guéry, *J. Electrochem. Soc.*, **157**, A641 (2010).
10. Y. Chen, C. Davoisne, J. M. Tarascon, and C. Guéry, *J. Mat. Chem.*, **22**, 5295 (2012).
11. Y. Z. Su, Y. C. Fu, Y. M. Wei, J. W. Yan, and W. B. Mao, *Chemphyschem*, **11**, 2764 (2010).
12. M. T. Alam, M. M. Islam, T. Okajima, and T. Ohsaka, *J. Phys. Chem. C*, **112**, 16600 (2008).
13. R. Atkin, S. Z. El Abedin, N. Borisenko, R. Hayes, L. H. S. Gasparotto, and F. Endres, *J. Phys. Chem. C*, **113**, 13266 (2009).
14. W. Zhou, S. Inoue, T. Iwahashi, K. Kanai, K. Seki, T. Miyamae, D. Kim, Y. Katayama, and Y. Ouchi, *Electrochem. Comm.*, **12**, 672 (2010).

15. S. Baldelli, *Accounts Chem. Res.*, **41**, 421 (2008).
16. Y. Katayama, H. Onodera, M. Yamagata, and T. Miura, *J. Electrochem. Soc.*, **151**, A59 (2004).
17. M. C. Buzzeo, O. V. Klymenko, J. D. Wadhawan, C. Hardacre, K. R. Seddon, and R. G. Compton, *J. Phys. Chem. A*, **107**, 8872 (2003).
18. R. G. Evans, O. V. Klymenko, S. A. Saddoughi, C. Hardacre, and R. G. Compton, *J. Phys. Chem. B*, **108**, 7878 (2004).
19. E. Azaceta, S. Chavhan, P. Rossi, M. Paderi, S. Fantini, M. Ungureanu, O. Miguel, H. J. Grande, and R. Tena-Zaera, *Electrochim. Acta*, **71**, 39 (2012).
20. E. Azaceta, R. Marcilla, D. Mecerreyes, M. Ungureanu, A. Dev, T. Voss, S. Fantini, H. J. Grande, G. Cabanero, and R. Tena-Zaera, *Phys. Chem. Chem. Phys.*, **13**, 13433 (2011).
21. V. Lair, J. Sirieix-Plenet, L. Gaillon, C. Rizzi, and A. Ringuedé, *Electrochim. Acta*, **56**, 784 (2010).
22. Z. L. Wang, *Mater. Sci. Eng. R*, **64**, 33 (2009).
23. T. Minami, T. Yamamoto, and T. Miyata, *Thin Solid Films*, **366**, 63 (2000).
24. J. Clatot, G. Campet, A. Zeinert, C. Labrugere, and A. Rougier, *Appl. Surf. Sci.*, **257**, 5181 (2011).
25. L. C. Nistor, C. Ghica, D. Matei, G. Dinescu, M. Dinescu, and G. Van Tendeloo, *J. Cryst. Growth*, **277**, 26 (2005).
26. F. Paraguay, W. Estrada, D. R. Acosta, E. Andradeb, and M. Miki-Yoshidac, *Thin Solid Films*, **350**, 192 (1999).
27. K. V. Gurav, U. M. Patil, S. M. Pawar, J. H. Kim, and C. D. Lokhande, *J. Alloy. Compd.*, **509**, 7723 (2011).
28. T. Mouet, T. Devers, A. Telia, Z. Messai, V. Harel, K. Konstantinov, I. Kante, and M. T. Ta, *Appl. Surf. Sci.*, **256**, 4114 (2010).
29. T. Yoshida, D. Komatsu, N. Shimokawa, and H. Minoura, *Thin Solid Films*, **451–452**, 166 (2004).
30. S. Peulon and D. Lincot, *J. Electrochem. Soc.*, **145**, 864 (1998).
31. D. Gal, G. Hodes, D. Lincot, and H. W. Schock, *Thin Solid Films*, **361–362**, 79 (2000).
32. T. Kawano and H. Imai, *J. Ceram. Soc. Jpn.*, **118**, 969 (2010).
33. B. E. Prasad and P. V. Kamath, *J. Solid State Electrochem.*, **14**, 2083 (2010).
34. S. Nénon, R. Méreau, S. Salman, F. Castet, T. Van Regemorter, S. Clima, D. Beljonne, and J. Cornil, *J. Phys. Chem. Lett.*, **3**, 58 (2012).
35. P. Waltereit, O. Brandt, A. Trampert, H. T. Grah, J. Meningen, M. Ramsteiner, M. Reiche, and K. H. Ploog, *Nature*, **406**, 865 (2000).
36. S. Y. Chu, T. Y. Chen, and W. Water, *J. Crystal Growth*, **257**, 280 (2003).
37. N. Serizawa, Y. Katayama, and T. Miura, *J. Electrochem. Soc.*, **156**, D503 (2009).
38. G. Sauerbrey, *Z. Phys.*, **155**, 206 (1959).
39. A. P. Abbott, J. C. Barron, G. Frish, K. S. Ryder, and A. F. Silva, *Electrochim. Acta*, **56**, 5272 (2011).
40. E. L. Smith, J. C. Barron, A. P. Abbott, and K. S. Ryder, *Anal. Chem.*, **81**, 8466 (2009).
41. J. T. Li, S. R. Chen, X. Y. Fan, L. Huang, and S. G. Sun, *Langmuir*, **23**, 13174 (2007).
42. P. Barpanda, J. N. Chotard, C. Delacourt, M. Reynaud, Y. Filinchuk, M. Armand, M. Deschamps, and J. M. Tarascon, *Angew. Chem. Int. Edit.*, **50**, 2526 (2011).
43. J. M. Tarascon, N. Recham, M. Armand, J. N. Chotard, P. Barpanda, W. Walker, and L. Dupont, *Chem. mater.*, **22**, 724 (2010).
44. M. M. Huang, Y. Jiang, P. Sasisanker, G. W. Driver, and H. Weingartner, *J. Chem. Eng. Data*, **56**, 1494 (2011).
45. P. Y. Chen and C. L. Hussey, *Electrochim. Acta*, **52**, 1857 (2007).